2014

Influence of Iron and Aeration on Staphylococcus aureus Growth, Metabolism, and Transcription

Nagender Ledala
University of Nebraska—Lincoln

Bo Zhang
University of Nebraska—Lincoln

Javier Seravalli
University of Nebraska—Lincoln, jseravalli1@unl.edu

Robert Powers
University of Nebraska-Lincoln, rpowers3@unl.edu

Greg Somerville
University of Nebraska—Lincoln, gsomerville3@unl.edu

JB
Journals.ASM.org

Influence of Iron and Aeration on *Staphylococcus aureus* Growth, Metabolism, and Transcription

Nagender Ledala,[a] Bo Zhang,[b] Javier Seravalli,[c] Robert Powers,[b] Greg A. Somerville[a]

School of Veterinary Medicine and Biomedical Sciences, University of Nebraska—Lincoln, Lincoln, Nebraska, USA[a]; Department of Chemistry, University of Nebraska—Lincoln, Lincoln, Nebraska, USA[b]; Department of Biochemistry, University of Nebraska—Lincoln, Lincoln, Nebraska, USA[c]

Staphylococcus aureus **is a prominent nosocomial pathogen and a major cause of biomaterial-associated infections. The success of *S. aureus* as a pathogen is due in part to its ability to adapt to stressful environments. As an example, the transition from residing in the nares to residing in the blood or deeper tissues is accompanied by changes in the availability of nutrients and elements such as oxygen and iron. As such, nutrients, oxygen, and iron are important determinants of virulence factor synthesis in *S. aureus*. In addition to influencing virulence factor synthesis, oxygen and iron are critical cofactors in enzymatic and electron transfer reactions; thus, a change in iron or oxygen availability alters the bacterial metabolome. Changes in metabolism create intracellular signals that alter the activity of metabolite-responsive regulators such as CodY, RpiRc, and CcpA. To assess the extent of metabolomic changes associated with oxygen and iron limitation, *S. aureus* cells were cultivated in iron-limited medium and/or with decreasing aeration, and the metabolomes were examined by nuclear magnetic resonance (NMR) spectroscopy. As expected, oxygen and iron limitation dramatically decreased tricarboxylic acid (TCA) cycle activity, creating a metabolic block and significantly altering the metabolome. These changes were most prominent during post-exponential-phase growth, when TCA cycle activity was maximal. Importantly, many of the effects of iron limitation were obscured by aeration limitation. Aeration limitation not only obscured the metabolic effects of iron limitation but also overrode the transcription of iron-regulated genes. Finally, in contrast to previous speculation, we confirmed that acidification of the culture medium occurs independent of the availability of iron.**

Staphylococcus aureus is a versatile pathogen capable of infecting almost any niche within a human or animal host. As with most bacterial pathogens, successful pathogenesis requires that *S. aureus* gain entry into a host (e.g., through a breach in the skin), adhere to a suitable surface, avoid being killed by the host's immune system, acquire nutrients, and proliferate. Notably, every step in this pathogenic process involves metabolic changes and/or metabolic regulation. Entry into a host is an environmental change that dramatically alters the availability of nutrients and cofactors. Similarly, the transition from synthesizing adhesins to producing tissue-damaging secreted virulence determinants is preceded by changes in the bacterial nutritional status (1). To avoid being killed by the host's immune system, *S. aureus* alters its metabolism to limit damage by oxidative and nitrosative stress (2). The act of acquiring nutrients is regulated by metabolite-responsive regulators that respond to changes in the bacterial metabolic status (3). Finally, proliferation is a carbon- and energy-intensive undertaking. In short, the success of *S. aureus* as a pathogen depends on its ability to meet the rapidly changing nutritional and energy requirements necessary for survival and proliferation within a host. The ability to meet the changing nutritional and energy requirements is complicated by the host, which limits access to enzymatic cofactors such as oxygen and iron by sequestering these cofactors in host proteins and molecules (e.g., hemoglobin, heme, and transferrin). The limited availability of these cofactors creates metabolic blocks that hinder virulence factor synthesis (4, 5), which leaves *S. aureus* vulnerable to the host's immune system.

The potential consequences of a metabolic block(s) (i.e., decreased fecundity and fitness and/or death) create selective pressure to maintain a functional metabolic state. Over time, this selective pressure has led to the evolution/acquisition of metabolite-responsive regulators (e.g., CodY, CcpA, and RpiRc) that maintain metabolic homeostasis when nutritional and environmental conditions are favorable and that facilitate metabolic adaptations when nutritional and environmental conditions change (6–8). Specifically, CodY responds to changes in branched-chain amino acids and GTP concentrations (9, 10), while CcpA indirectly responds to glucose-6-phosphate and fructose-1,6-bisphosphate (11). While the RpiR regulators all have sugar isomerase binding domains, the metabolites that modulate their activities have yet to be determined (8). These metabolite-responsive regulators, i.e., CodY, CcpA, and RpiRc, coordinate both virulence determinant biosynthesis and metabolism in staphylococci (8, 9, 12). In general, the activity of metabolite-responsive regulators is controlled by intracellular concentrations of numerous compounds, such as biosynthetic intermediates (13), amino acids (14), nucleic acids (15), and cofactors (e.g., iron) (16). In *Staphylococcus epidermidis*, the intracellular concentrations of metabolites can be altered by environmental stressors such as antibiotics, ethanol, metal ion limitation, or nutrient depletion (3, 17, 18). This creates a mechanism by which extracellular stress can be transduced into intracellular metabolic signals that elicit regula-

Received 21 January 2014 **Accepted** 28 March 2014
Published ahead of print 4 April 2014
Address correspondence to Greg A. Somerville, gsomerville3@unl.edu.
N.L. and B.Z. are equal contributors.
Supplemental material for this article may be found at http://dx.doi.org/10.1128/JB.01475-14.

doi:10.1128/JB.01475-14

tory changes via metabolite-responsive regulators. While the transduction of external factors into internal metabolic signals has been demonstrated in *S. epidermidis*, it has not been shown in *S. aureus*.

Two important enzymatic cofactors that influence *S. aureus* fitness and that are controlled by the host are oxygen and iron. Numerous studies have shown that oxygen and iron availability can influence growth, antibiotic tolerance, and the synthesis of virulence factors (19–23); however, little regard has been given to the metabolic changes that accompany iron and oxygen limitation (24–26). Where the metabolic effects of iron or oxygen limitation have been examined, those studies addressed only the metabolic effects of a single stress and in a single growth phase/state. The analysis of a single growth phase/state overlooks the fact that staphylococci have two very distinct metabolic states that correlate with the exponential and post-exponential growth phases (27). Because pathogenic bacteria rarely encounter a single stress, we chose to examine the effect of combined stresses of iron and oxygen limitation on exponential- and post-exponential-phase metabolomes. In addition, we also assessed the contributions of single stresses (i.e., iron or oxygen limitation) to the overall effects of combined stresses (i.e., iron and oxygen limitation). Finally, by analyzing the metabolic effects of single stresses, we can identify common metabolic signals, similar to what was done with *S. epidermidis* (17, 18). In the current study, the effects of oxygen and iron limitation on the metabolome of *S. aureus* strain SA564 were examined by using nuclear magnetic resonance (NMR) metabolomics. In addition, a select set of genes was examined for transcriptional changes that might be associated with the altered growth conditions.

MATERIALS AND METHODS

Bacterial strains, media, and cultivation conditions. *S. aureus* strain SA564 was grown in tryptic soy broth (TSB; BD Biosciences) or on tryptic soy agar (TSA). For iron limitation cultivation conditions, deferrated TSB (DTSB) medium was used (17). In this study, iron-limited medium was preferred over "iron-free" medium because iron-free medium requires the addition of adulterants such as deferoxamine mesylate. These adulterants are added to chelate iron; however, they also chelate other cations (28), which makes comparisons between cultivation conditions impractical because more than one variable would be changed. To prevent pyrolysis of labile metabolites, DTSB and TSB were prepared by filter sterilization. For iron-limiting conditions, bacterial cultures were grown overnight in 10 ml of DTSB, harvested by centrifugation at 3,795 × *g*, washed once in 10 ml of DTSB, and suspended in fresh DTSB. This culture was used to inoculate the starter cultures at a 1:100 dilution, and the starter cultures were cultivated in 100 ml of DTSB or TSB for 2 h. After 2 h of growth, these cultures were used to inoculate the primary cultures to an optical density at 600 nm (OD_{600}) of 0.06. Each primary culture was cultivated in prewarmed DTSB or TSB at defined flask-to-medium ratios. All cultures were grown at 37°C with constant aeration (225 rpm) and growth (OD_{600}), and pHs were measured at hourly intervals for 12 h. For the purpose of changing culture aeration during growth, flask-to-medium ratios (vol/vol) of 10:8, 10:4, 10:2.5, and 10:1 were used. This approach takes advantage of the poor coefficient of diffusion of oxygen into water to alter the amount of oxygen available to the bacteria (29).

Sample preparation for NMR metabolomic analysis. Bacterial cultures were harvested during the exponential (2 h) and post-exponential (6 h) growth phases. For one-dimensional (1D) ^{1}H NMR experiments, eight biological replicates (10 OD_{600} units each) were harvested for each cultivation condition and growth phase. For two-dimensional (2D) ^{1}H-^{13}C heteronuclear single quantum coherence (HSQC) experiments, four biological replicates (20 OD_{600} units each) were harvested for each cultivation condition and growth phase. Bacteria were harvested by using a sterile 0.45-μm Microfil V filtration system (EMD Millipore Corporation) that had been prewashed with 5 ml of sterile phosphate-buffered saline (PBS) (pH 7.4). Following filtration, bacteria were washed twice with 5 ml of ice-cold PBS, and each membrane was transferred into a 50-ml conical tube and quenched in liquid nitrogen. After quenching, the conical tubes were placed in ice, and bacteria were collected from the filter by using ice-cold 20 mM phosphate buffer (1 ml). The bacterial suspensions were normalized to equal OD_{600} units (10 for 1D NMR and 20 for 2D NMR) in a 1-ml total volume, transferred into lysing matrix B tubes, and lysed twice (speed 6 for 40 s) by using a FastPrep FP120 instrument (MP Biomedicals). The samples were rested on ice for 5 min between lysings. To remove cell debris and glass beads, samples were centrifuged at 17,000 × *g* for 2 min at −9°C, and 700 μl of the supernatant from each tube was transferred into a new 2-ml microcentrifuge tube (precooled to −20°C). One milliliter of ice-cold phosphate buffer was added to the residual sample in the lysing matrix B tubes, mixed, and centrifuged. After the second centrifugation, 900 μl of the supernatant from each tube was pooled with the samples from the first centrifugation. Of the 1.6-ml volume for each sample, 100 μl was removed, and the protein concentration was determined by using a modified Lowry assay kit (Thermo Fisher Scientific). The remaining 1.5 ml of each sample was lyophilized, and 600 μl of D_2O was added prior to analysis. A total of 50 μM 3-(trimethylsilyl)propionic acid-2,2,3,3–d4 (TMSP-d4) or 500 μM TMSP-d_4 (Sigma-Aldrich) was added to each sample as the internal standard for 1D ^{1}H NMR or 2D ^{1}H-^{13}C HSQC experiments, respectively.

Data collection. 1D data collection was performed as described previously (30), while 2D time zero extrapolated ^{1}H-^{13}C HSQC ($HSQC_0$) NMR spectra were processed as described previously (31). For each sample, a total of 1,024 data points with a spectrum width of 10.00 ppm in the ^{1}H dimension and a total of 64 data points with a spectrum width of 140.00 ppm in the ^{13}C dimension were collected. A total of 16 dummy scans and 64 scans with a receiver gain of 9,195.2 and a relaxation delay of 1.5 s were applied for each sample.

Data analysis. 1D ^{1}H NMR spectra were processed as described previously (18). 2D ^{1}H-^{13}C HSQC spectra were processed by using the NMRPipe software package (32). Peak picking and peak matching were done by using NMRViewJ version 8 (33). A table of peaks along with the respective intensities were recorded, and the concentrations of metabolites were calculated by using a standard curve generated by using nine metabolites with known concentrations [D-glucose-$^{13}C_6$, D-fructose-$^{13}C_6$, glycine-$^{13}C_2$, DL-alanine-3-^{13}C, sodium pyruvate-$^{13}C_3$, succinic acid-$^{13}C_4$, sodium acetate-$^{13}C_2$, 2-keto-3-(methyl-^{13}C)-butyric acid-4-^{13}C, sodium salt, and 2-ketobutyric acid-4-^{13}C sodium salt hydrate (Sigma-Aldrich)] (31). A Student *t* test was used to determine the statistical significance ($P < 0.05$) of metabolite concentration changes.

The principal component analysis (PCA) and orthogonal projections to latent structures-discriminant analysis (OPLS-DA) score plots and the shared and unique structure (SUS) plots were generated by using the SIMCA 12.0+ statistical package (Umetrics). The OPLS-DA models were validated by using a modified leave-one-out method (34, 35) and analysis of variance of cross-validated residuals (CV-ANOVA) (36). The metabolomics tree diagrams (dendrograms) and the ellipses corresponding to the 95% confidence limits from a normal distribution for each cluster within the PCA score plots were generated by using our PCA/PLS-DA utilities (http://bionmr.unl.edu/pca-utils.php) (37, 38).

Data interpretation. The peaks were assigned to metabolites by using chemical shift references from the Human Metabolomics Database (HMDB) (39), the Platform for RIKEN Metabolomics (PRIMe) (40), the Biological Magnetic Resonance Data Bank (BMRB) (41), and Chenomx NMR Suite 7.6 software (Chenomx, Inc., Edmonton, Canada). Heat maps were generated in R with a gplots package (42).

ICP-MS analysis of DTSB. Cultivation of *S. aureus* strain SA564 was performed as described above. For the determination of iron concentrations in the culture supernatants, 1 ml of each culture was harvested dur-

TABLE 1 Real-time RT-PCR primers used in this study

Primer	Mu50 ORF[a]	Sequence
16SrRNA RTF	SAVrRNA16	CGTGCTACAATGGACAATACAAA
16SrRNA RTF	SAVrRNA16	ATCTACGATTACTAGCGATTCCA
citB RTF	SAV1350	GCGCAACAGCAACTGATTTA
citB RTR	SAV1350	GTTGTACACCTGGACCAAAGA
feoB RTF	SAV2584	GGAATGACAGCAACACAGTTAC
feoB RTR	SAV2584	GTGCTGACTGACCACCTAAA
sbnA RTF	SAV0116	TTCTGTAGGGCAAACACCTATG
sbnA RTR	SAV0116	GCTGCCTCCAGGATTCATATAC
sstC RTF	SAV0735	GACCTAATGGTGCGGGTAAG
sstC RTR	SAV0735	CAGACATGAGCTGTCCATCTATT

[a] Gene designations based on the *Staphylococcus aureus* strain Mu50 genomic DNA sequence (68). ORF, open reading frame.

ing the exponential (2 h) or post-exponential (6 h) growth phase by centrifugation at 3,795 × *g* for 5 min at room temperature. To remove any residual bacteria, samples were passed through Nalgene 0.2-μm polyethersulfone membrane syringe filters (Thermo Fisher Scientific). All samples were diluted 1:20 with a solution containing 52.6 ppb ^{71}Ga in 0.1% HNO_3, which resulted in a ^{71}Ga concentration of 50 ppb, which was used as an internal standard. Inductively coupled plasma mass spectrometry (ICP-MS) analyses were performed at the University of Nebraska—Lincoln Spectroscopy Core Facility by using an Agilent Technologies ICP-MS 7500cs instrument with an ESI SC-4 high-throughput autosampler (Elemental Scientific, Inc.). The concentration of metals was calculated by using ChemStation for ICP software with a calibration curve for 18 elements from serial dilutions of a standard stock from Inorganic Ventures. The instrument was operated with an octopole collision reaction cell filled with He at a flow rate of 5.0 ml/min and the following Ar plasma conditions: plasma power of 1,500 W, plasma gas at 17 liters/min, auxiliary gas at 1 liter/min, sample gas at 0.9 to 1.1 liters/min, makeup gas at 0.1 to 0.2 liters/min, and a sample flow rate of 0.1 ml/min. For each sample, three replicates from three independent cultures were analyzed. Statistical significance was determined by one-way ANOVA using SigmaPlot 11.2 software (Systat Software, Inc.).

Aconitase activity assay. Aconitase enzymatic activity was measured as described previously (17). Protein concentrations were determined by using a modified Lowry protein assay kit (Thermo Fisher Scientific).

Real-time quantitative RT-PCR (qRT-PCR). Total RNA was isolated from 10 OD_{600} units of bacteria harvested in the exponential (2 h) and post-exponential (6 h) growth phases by using the FastRNA Pro Blue kit (MP Biomedical) and the RNeasy kit (Qiagen), as described previously (43). For mRNA analysis, a two-step real-time reverse transcription-PCR (RT-PCR) was performed with cDNA synthesis from total RNA followed by PCR. Ten micrograms of Turbo DNase (Bio-Rad)-treated total RNA for each sample was used to prepare cDNA by a reverse transcriptase reaction using iScript master mix (Bio-Rad) according to the manufacturer's protocol. The reaction mixtures for real-time PCR contained 10 μl of 2× SsoAdvanced SybrGreen Supermix (Bio-Rad), 7 pmol of each primer (Table 1), and 5 μl of 10-fold-diluted cDNA, in a total volume of 20 μl. As an internal reference, primers for 16S rRNA were used in the same reaction volume containing 1,000-fold-diluted cDNA as a template. The real-time PCR cycling conditions were an initial denaturation step at 94°C for 3 min, followed by 40 cycles at 94°C for 15 s, 60°C for 25 s, and 72°C for 20 s. Relative transcript levels were determined by the comparative threshold ($\Delta\Delta C_T$) method (Bio-Rad). Experimental setup and data analysis were carried out by using a CFX96 real-time PCR detection system and Bio-Rad CFX Manager software version 3.0 (Bio-Rad).

Determination of acetate, glucose, and lactate levels in medium supernatant. Metabolite concentrations in the culture media were determined by using kits purchased from R-biopharm, Inc.

RESULTS

Growth of *S. aureus* under conditions of iron and oxygen limitation. The transition from an oxygen- and iron-replete environment (e.g., the skin and the nares) to an oxygen- and iron-limited environment (e.g., blood) constrains metabolic possibilities because many enzymatic reactions require iron and oxygen as cofactors. These constraints have fitness consequences, specifically the ability to place progeny into the next generation (44–46). To assess the extent of the fitness cost of iron and oxygen limitation on growth yield, *S. aureus* strain SA564 was cultivated under iron- and/or oxygen-limited conditions, and growth was monitored (Fig. 1A and B). As expected, the growth rates were largely independent of iron- and/or oxygen-limited conditions. Consistent with the Pasteur effect (47), oxygen-limited growth conditions dramatically decreased biomass generation, whereas iron limitation did not significantly alter the biomass generated per mmol of glucose (Fig. 1C). Importantly, these data demonstrate the ease with which a batch culture can become microaerobic/anaerobic at an atmospheric oxygen concentration of 20.946% (29) and with vigorous agitation at 225 rpm. This transition to a microaerobic/anaerobic status is due to two factors: first, the poor diffusion coefficient for oxygen into water, and second, the relatively small surface area that is exposed to atmospheric oxygen as the volume of medium in a culture flask is increased. In contrast to oxygen limitation, iron limitation decreased the growth yield of strain SA564 by only ~25% relative to growth in iron-replete culture medium (Fig. 1A). In *S. aureus*, the demand for iron is greatest in the post-exponential growth phase (5), when the tricarboxylic acid (TCA) cycle and the electron transport chain are most active; hence, the small amount of iron in the culture medium (Fig. 1B) is sufficient to maintain the exponential growth rate but not the growth yield (Fig. 1A).

S. aureus is a facultative anaerobe and is well adapted for growth in low-oxygen environments when nutrients are abundant. As nutrients become scarce, *S. aureus* catabolizes incompletely oxidized carbon compounds (e.g., lactic acid or acetic acid) that accumulate in the medium during the exponential growth phase (27); hence, the pH of the culture medium will alkalinize. As expected, strain SA564 grown under oxygen- and iron-replete conditions began to alkalinize the culture medium during the transition from the exponential growth phase to the post-exponential growth phase (Fig. 1D). Iron-limited growth slightly delayed and decreased the alkalinization of the culture medium, while oxygen limitation severely restricted alkalinization of the medium.

In contrast to previous speculation, iron limitation does not lead to the acidification of the culture medium (26). As stated above, the acidification of the culture medium is the result of the inefficient use of carbohydrates during growth under nutrient-rich conditions, which occurs irrespective of the availability of iron or oxygen (Fig. 1C to F). The decreased ability of oxygen-limited cultures and, to a lesser extent, iron-limited cultures to alkalinize the medium was most likely due to a diminished capacity to catabolize organic acids and amino acids. To address this possibility, the concentrations of acetic acid and lactic acid in the culture media were measured throughout the growth cycle (Fig. 1E and F). During microaerobic/anaerobic growth (i.e., when the flask-to-medium ratio is 10:8), pyruvate is largely reduced to lactic acid (48, 49) (Fig. 1F). In contrast, when the flask-to-medium

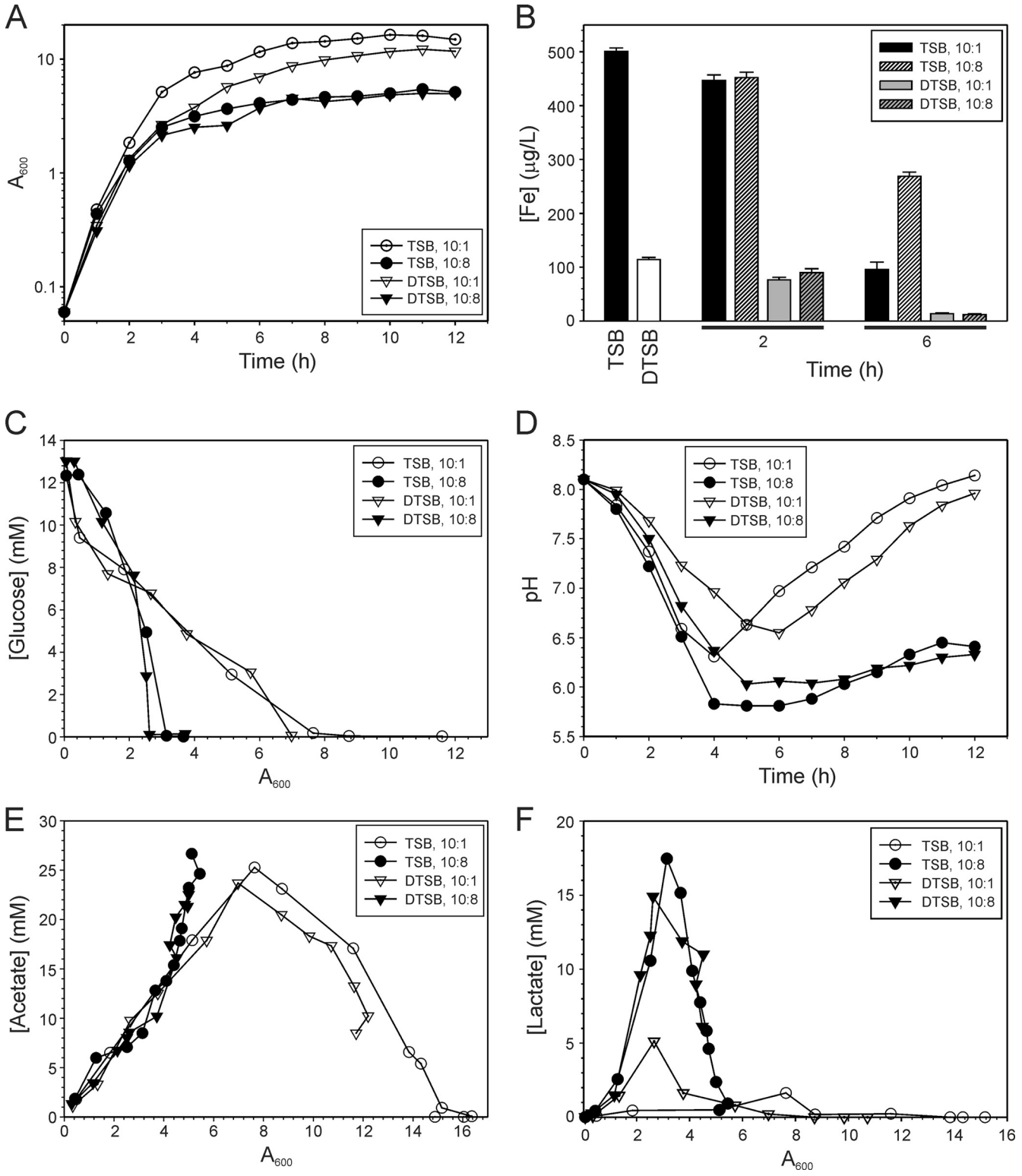

FIG 1 Cultivation of *S. aureus* strain SA564 under aeration- and/or iron-limiting conditions. (A) Growth curves. (B) Iron concentrations of uninoculated media and cultivation media harvested in the exponential and post-exponential growth phases. (C) Glucose utilization as a function of growth. (D) pH profiles. (E) Acetate accumulation and depletion in culture media. (F) Lactate accumulation and depletion in culture media. Data are representative of experiments performed at least twice. The data in panel B are presented as the means of 3 independent experiments done in triplicate, with error bars representing standard deviations. TSB, tryptic soy broth; DTSB, deferrated TSB. Flask-to-medium ratios were 10:1 (aerobic) and 10:8 (microaerobic/anaerobic).

ratio was altered to 10:1, pyruvate was oxidized to acetyl coenzyme A (acetyl-CoA) and CO_2 by the pyruvate dehydrogenase complex (50) (Fig. 1E). In the exponential growth phase, acetyl-CoA is used to generate the small phospho-donor acetyl-phosphate, which serves as a substrate for acetate kinase in substrate-level phosphorylation to generate ATP and acetic acid (Fig. 1E). During the post-exponential growth phase, this acetic acid can be used for the synthesis of acetyl-CoA to fuel the TCA cycle. When iron was limiting, the catabolism of acetate and the biomass generated from that catabolism were reduced (Fig. 1E). As expected, oxygen limitation inhibited the catabolism of acetate; however, it had only a slight effect on lactate catabolism (Fig. 1E and F). The latter data were surprising because acetate catabolism through the TCA cycle (27) and lactate catabolism through L-lactate-quinone oxidoreductase (Lqo) (51) both require electron acceptors to balance the redox status.

Iron and oxygen limitations create metabolic blocks. Staphylococci lack a glyoxylate shunt and catabolize acetate through the TCA cycle (27, 52); hence, a diminished ability to catabolize acetate (Fig. 1E) suggests that the TCA cycle had reduced activity under iron- and oxygen-limited growth conditions. To test this suggestion, the TCA cycle enzyme aconitase was assayed for activity under iron- and oxygen-limited growth conditions (Fig. 2A and B). Since aconitase is an iron-sulfur cluster-containing enzyme, iron limitation would be expected to decrease its activity. As expected, growth of *S. aureus* strain SA564 in iron-limited culture medium dramatically decreased post-exponential-growth-phase aconitase activity (Fig. 2A). As stated above, one function of iron is to facilitate electron transfer reactions, a process that requires an electron donor (e.g., NADH and NADPH) and an electron acceptor (e.g., oxygen). In the presence of iron but in the absence of an electron acceptor, reduced dinucleotides will accumulate, which should inhibit enzyme activity through a feedback mechanism. To test this hypothesis, we limited oxygen availability by changing the flask-to-medium ratio and assayed for aconitase activity (Fig. 2B) (29). As the medium volume was increased, the surface area available for oxygen diffusion decreased, resulting in a post-exponential-growth-phase decrease in aconitase activity. While aconitase is an excellent metabolic sentinel, iron and oxygen limitation will affect the activity of many enzymes in bacteria.

Iron and/or oxygen limitation alters the *S. aureus* metabolome. Iron- and oxygen-limited growth created a metabolic block at aconitase in the TCA cycle (Fig. 2A and B); however, these stresses also inhibit the activities of many different metabolic enzymes and pathways. It is impractical to assay for all enzymes that might be affected by iron- and/or oxygen-limited growth, so metabolic changes were assessed by using NMR metabolomics (Fig. 3). As expected, principal component analysis (PCA) of exponential-growth-phase metabolomes revealed that they were minimally affected by iron limitation, whereas oxygen limitation caused modest changes in the metabolomes (Fig. 3A and C). The heterogeneity of the exponential-growth-phase metabolomes is easily demonstrated in a PCA shared and unique structure (SUS) plot, where very few shared or inversely shared metabolites were identified (Fig. 3E). In contrast to the exponential growth phase, iron limitation significantly altered the post-exponential-growth-phase metabolome PCA score plot (Fig. 3B, D, and F). Similarly, oxygen limitation had a very pronounced effect on the metabolome. Interestingly, strain SA564 metabolomes from cultures

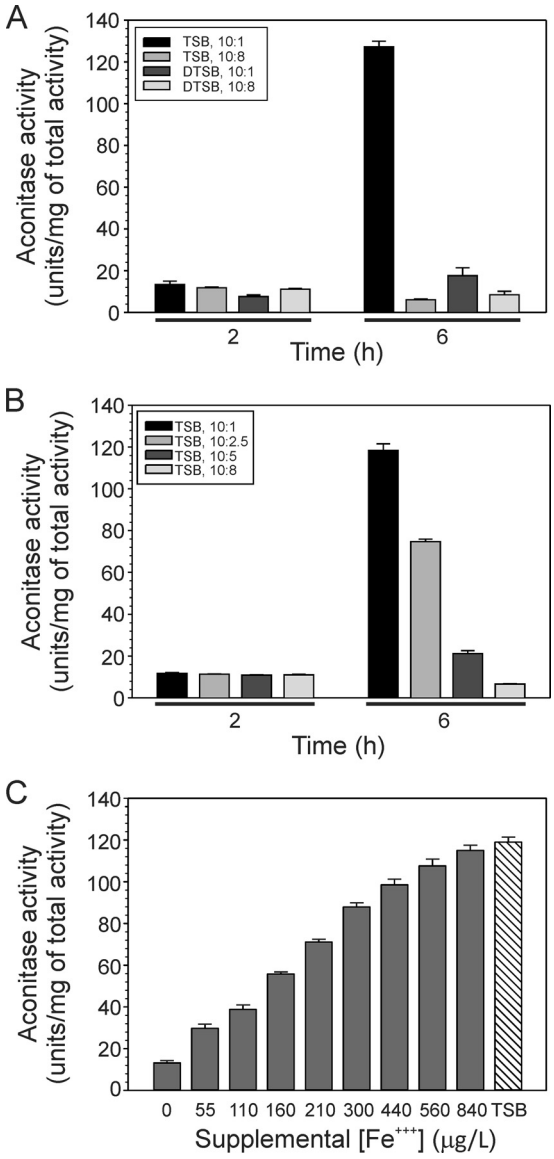

FIG 2 Temporal and stress-related aconitase activity differences in *S. aureus* strain SA564 in the exponential (2 h) and post-exponential (6 h) growth phases. (A) Aconitase activity during iron-limited growth. (B) Aconitase activity with decreasing aeration flask-to-medium ratios of 10:8, 10:5, 10:2.5, and 10:1. (C) Addition of iron to DTSB medium restores aconitase activity.

grown in iron-limited medium and with reduced aeration clustered more closely to the aeration-limited cultures than to the iron-limited cultures in a PCA score plot (Fig. 3B). In other words, the effect of iron limitation was masked by growth under conditions that limit the diffusion of oxygen into the culture medium. This can also be easily seen in the metabolic heat map, where the metabolic changes in post-exponential-growth-phase (6 h) cultures grown under conditions of aeration limitation are very similar, irrespective of iron limitation (Fig. 4). Taken together, these data demonstrate that the significance of iron limitation in *S. aureus* metabolism is determined largely by the growth phase and the availability of oxygen.

To identify metabolites that contributed to the separation of the sample clusters, OPLS-DA was employed (see Fig. S1 and S2 in

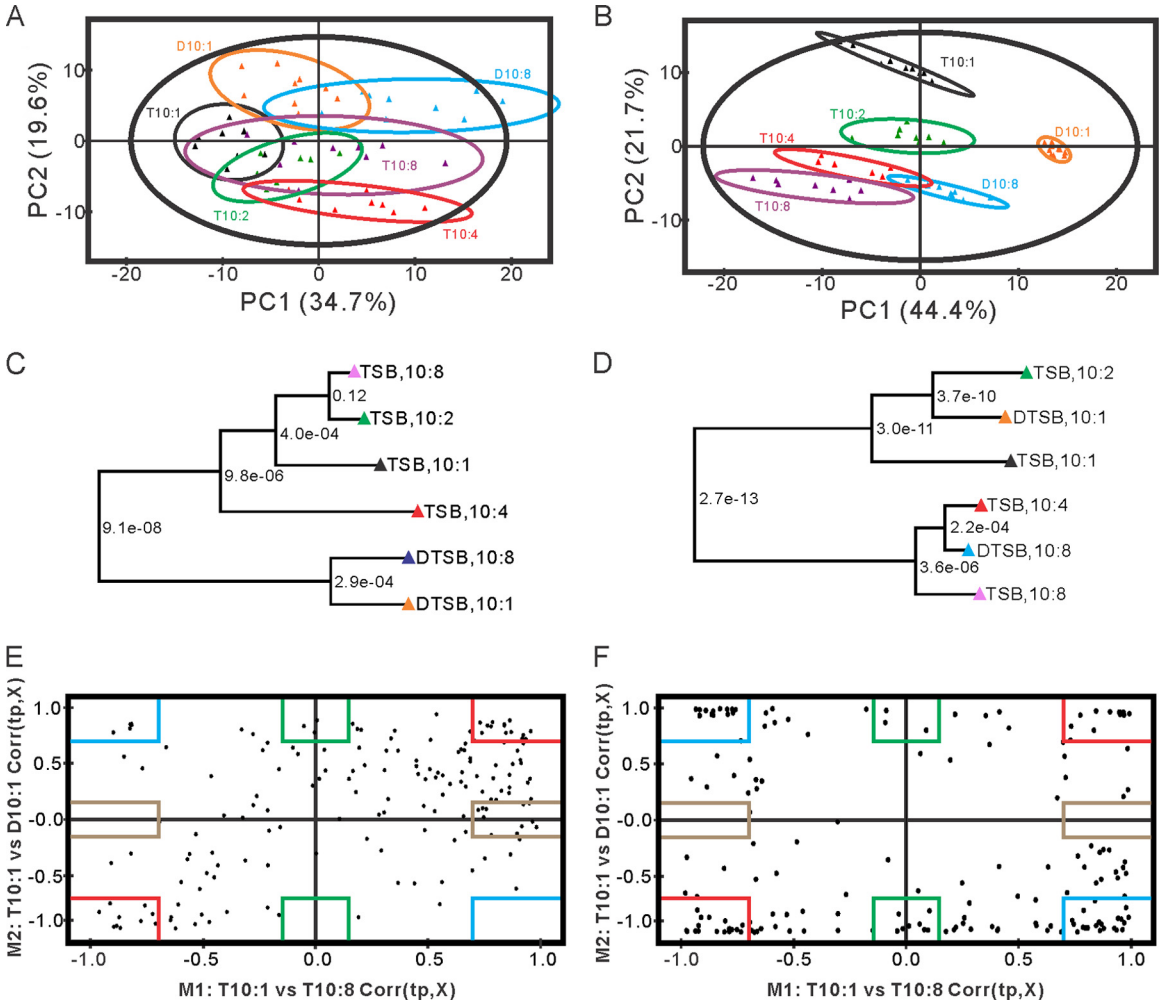

FIG 3 Exponential- and post-exponential-growth-phase metabolomic changes associated with iron- and/or oxygen-limited cultivation. (A and B) PCA score plots of the exponential (A) and post-exponential (B) growth phases of iron- and/or oxygen-limited cultures of *S. aureus* strain SA564. The ellipses in the PCA score plots correspond to the 95% confidence limits from a normal distribution for each cluster. (C and D) Metabolic tree generated by using the PCA score plot data demonstrating the relationship of iron- and/or oxygen-limited cultures in the exponential growth phase (C) and post-exponential growth phase (D). The statistical significance of each node in the metabolic tree is indicated by a *P* value. (E and F) Shared and unique structure (SUS) plots generated from the PCA model of the exponential (E) and post-exponential (F) growth phases comparing the classes of DTSB at a 10:1 ratio and TSB at 10:8 to a common reference (TSB, 10:1). The red boxes highlight the chemical shift bins with intensity changes that are shared by both models. The blue boxes highlight the chemical shift bins with intensity changes that are negatively shared by both models (relative intensity changes are in the opposite direction). The brown boxes highlight the chemical shift bins with intensity changes unique to model 1 (TSB at 10:8 versus TSB at 10:1). The green boxes highlight the chemical shift bins with intensity changes unique to model 2 (DTSB at 10:1 versus TSB at 10:1). In the post-exponential growth phase, 73 bins were found to be present in the shared/inversely shared region of the plot, compared to 29 bins found in the same regions in the exponential phase. The flask-to-medium ratios were 10:1 (aerobic) and 10:8 (microaerobic/anaerobic).

the supplemental material). In contrast to PCA, OPLS-DA is a supervised classification analysis where all the variation leading to separation between the two groups is aligned in the *x* axis (Pp) and all other variation is aligned in the *y* axis (Po) (53). To achieve separation based on aeration in an OPLS-DA scoring plot, clusters of TSB at a 10:1 dilution and DTSB at 10:1 were assigned a value of 0, and clusters of TSB at 10:8 and DTSB at 10:8 were assigned a value of 1 (see Fig. S1 in the supplemental material). This model resulted in one predictive and two orthogonal (1 + 2) components with a cross-validated predictive ability of $Q^2(Y) = 0.883$, which indicated that the data fit well within the model. The model was validated with CV-ANOVA, producing a statistically significant *P* value of 8.27×10^{-12}. Based on this model, the perturbations caused by iron limitation were largely suppressed when aeration was also limiting. As expected, the majority of the metabolic differences between aerobic growth and oxygen-limited growth include fermentation products, metabolites of pyruvate homeostasis, and amino acids (see Fig. S1 in the supplemental material). To achieve separation based on iron availability in an OPLS-DA score plot, clusters of TSB at 10:1 and TSB at 10:8 were assigned a value of 0, and clusters of DTSB at 10:1 and DTSB at 10:8, were assigned a value of 1 (see Fig. S2 in the supplemental material). This model also produced an excellent fit that resulted in one predictive and three orthogonal (1 + 3) components with a cross-validated predictive ability of $Q^2(Y) = 0.969$ (see Fig. S2 in the supplemental material). This

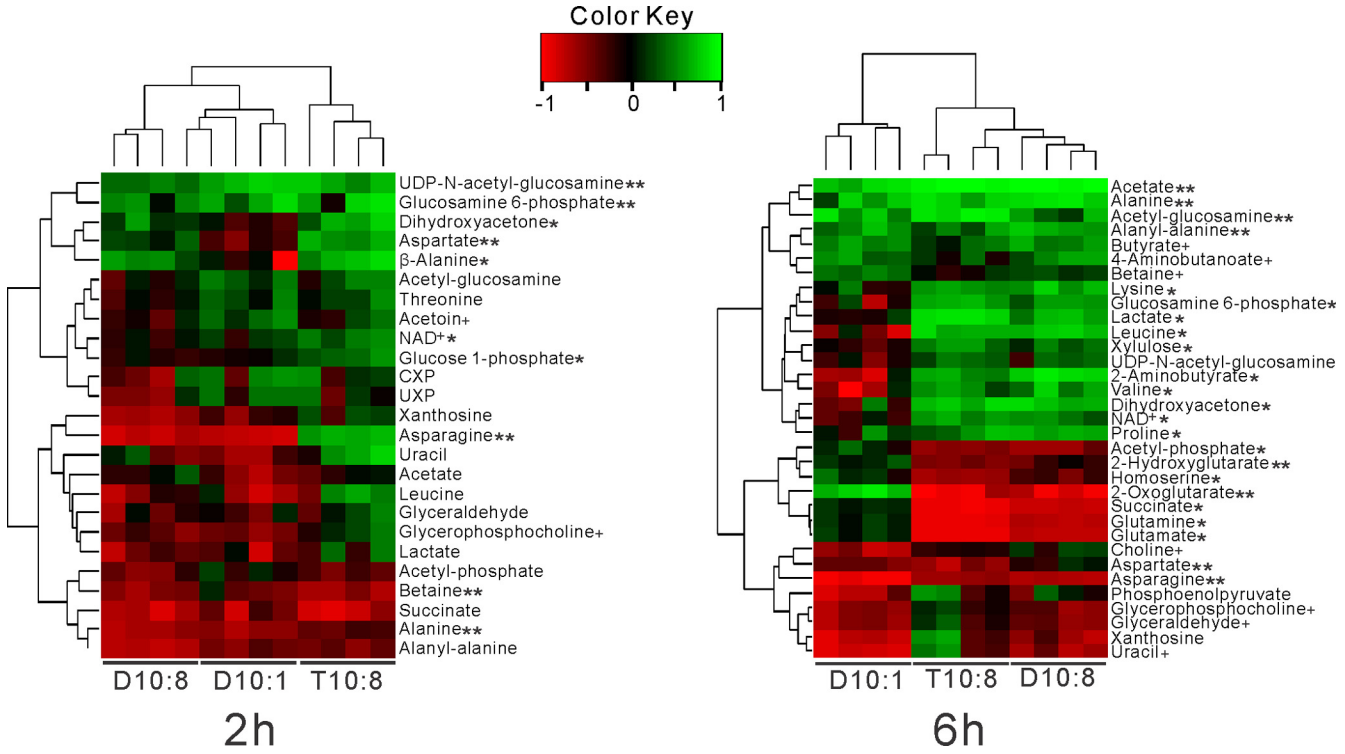

FIG 4 Heat maps showing the changes in metabolites as a function of cultivation conditions and growth phase. Culture media were TSB (tryptic soy broth) and DTSB (deferrated TSB). Flask-to-medium ratios were 10:1 (aerobic) and 10:8 (microaerobic/anaerobic). Statistical significance ($P < 0.05$) is indicated by ** (both oxygen and iron limitation), * (only oxygen limitation), and + (only iron limitation).

model was also validated by CV-ANOVA, producing a statistically significant P value of 1.33×10^{-17}. In this model, the four metabolomic clusters are largely separated from each other, suggesting that oxygen limitation as a stressor cannot be overwhelmed by iron limitation. Altogether, the clustering of metabolomes in both models suggested that the effects of iron limitation were suppressed by oxygen limitation.

Iron-regulated gene transcription varies with oxygen availability. If oxygen limitation can mask metabolic changes associated with iron limitation, it raises the question as to whether iron-dependent transcriptional changes can be obscured by oxygen limitation. To address this question, bacteria were grown under iron- and/or oxygen-limited culture conditions, and transcriptional changes in genes regulated by iron were assessed by using qRT-PCR (Fig. 5). As a positive control, transcription of the aconitase gene *acnA* (also known as *citB*) was assessed and compared to the enzyme activity data (Fig. 2A). Overall, the *acnA* mRNA levels correlated well ($r = 0.83$) with the enzymatic activity data. Similar to the metabolomics data, oxygen limitation was able to mask the effect of iron-limited growth on some genes. Specifically, oxygen limitation dramatically decreased the exponential-growth-phase (2 h) and post-exponential-growth-phase (6 h) transcription of the ferrous iron transporter *feoB* and the first gene (i.e., *sbnA*) of the staphyloferrin B biosynthetic locus (54). This reduction in transcript levels occurred despite the fact that the culture medium was iron limited (Fig. 1B). In contrast to *feoB* and *sbnA*, some genes (e.g., *sstC*, which codes for an ATP binding cassette in a siderophore transporter [55]) had only minimal changes in mRNA levels under iron- and/or oxygen-limited growth conditions. These data demonstrate that iron-dependent regulation of transcription in *S. aureus* can be suppressed under conditions of low oxygen availability. In addition, these data highlight the necessity of carefully considering, and reporting, bacterial cultivation conditions (29).

DISCUSSION

When cultures of *Staphylococcus epidermidis* are challenged with ethanol, antibiotics, iron limitation, or high glucose concentrations, these stresses cause common phenotypic changes; namely, they favor biofilm formation and/or biosynthesis of polysaccharide intercellular adhesin (56–59). These same stresses cause the post-exponential-growth-phase metabolomic profiles to resemble that of an *S. epidermidis* TCA cycle mutant (17, 18). The fact that divergent environmental challenges produce similar metabolic and phenotypic alterations suggests that common regulatory changes are occurring to produce the similar phenotypic outcomes (3). This suggestion was confirmed when it was observed that an *S. epidermidis ccpA* mutant failed to respond to metabolic changes associated with TCA cycle stress (7). Similar to *S. epidermidis*, we hypothesize that divergent environmental stresses cause common metabolic changes in *S. aureus* that alter the activity of metabolite-responsive regulators. The first step in identifying metabolite-responsive regulators is to define the common metabolic changes associated with environmental stresses (Fig. 4 and 6). The metabolic effects of many of the environmental stresses that *S. aureus* encounters have been studied in detail but with little, or no, deference to the temporal nature and the interconnectedness of metabolic changes (26, 60–62). The intent of the current study was

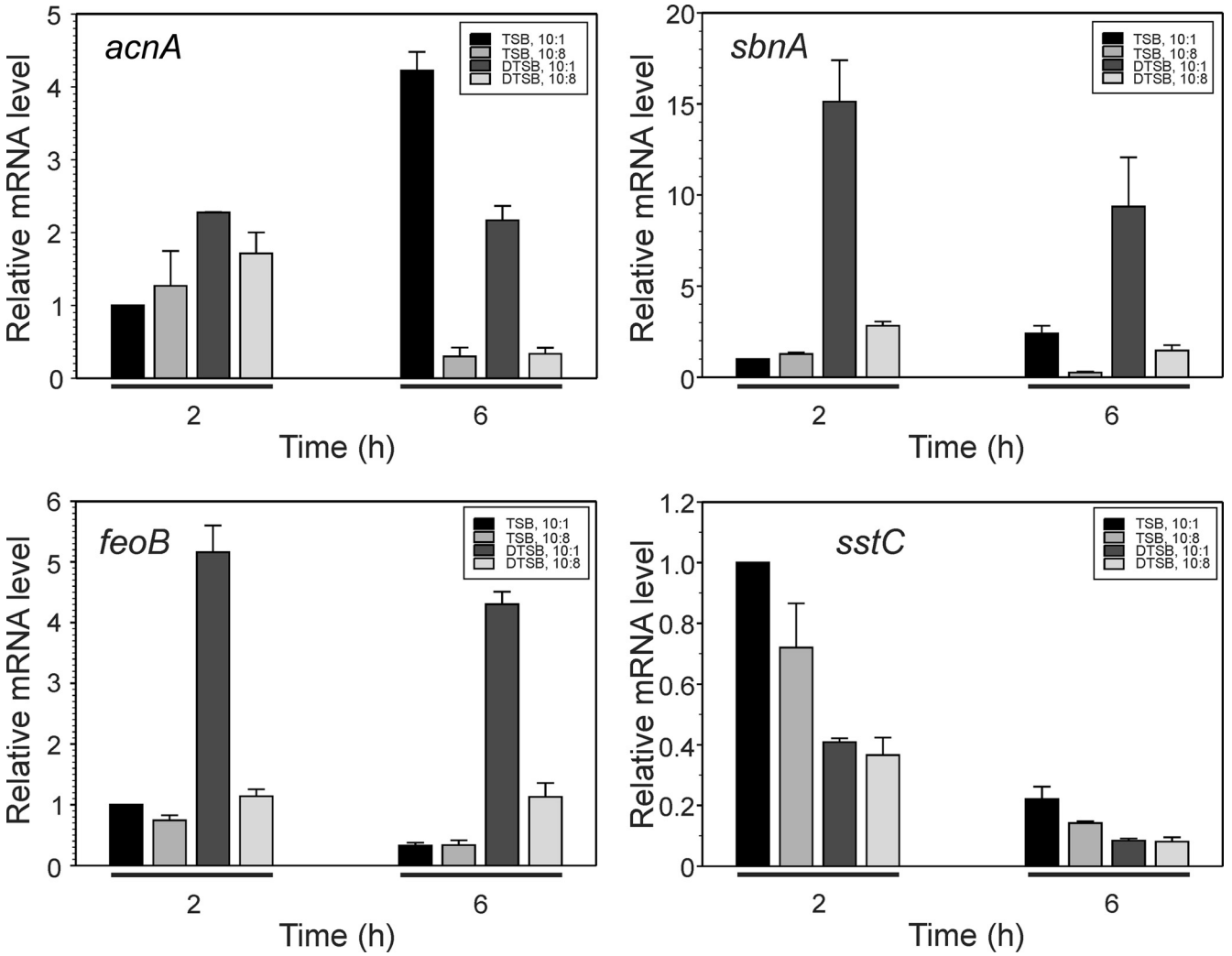

FIG 5 Oxygen limitation influences transcription of iron-regulated genes in the exponential (2 h) and post-exponential (6 h) growth phases. Relative mRNA levels for *acnA*, *sbnA*, *feoB*, and *sstC* were determined by qRT-PCR. The data are the means and standard errors of the means of at least 2 biological replicates, each determined in duplicate. Culture media were TSB (tryptic soy broth) and DTSB (deferrated TSB). Flask-to-medium ratios were 10:1 (aerobic) and 10:8 (microaerobic/anaerobic).

to identify common metabolic changes associated with iron and/or oxygen limitation that could alter the activity of metabolite-responsive regulators; the identification of these regulators is an active area of research in our laboratories. As a side benefit, this study reinforces the necessity of carefully considering and reporting cultivation conditions (63).

While the most prominent metabolomic differences are in the post-exponential growth phase, the exponential-growth-phase changes are greatest under conditions of combined iron- and oxygen-limited growth (Fig. 3, 4, and 6). For example, both iron and oxygen limitation redirect carbon into amino sugar biosynthesis (e.g., UDP-*N*-acetylglucosamine, glucosamine-6-phosphate, and acetyl-glucosamine). This redirection of carbon appears to be at the expense of the exponential-growth-phase basal-level TCA cycle carbon flow because the concentration of succinate is decreased relative to that under iron- and oxygen-replete growth conditions (Fig. 4 and 6). We observed a similar redirection of carbon into amino sugar biosynthesis in *S. epidermidis*, where TCA cycle stress induces the formation of an *N*-acetylglucosamine polymer known as polysaccharide intercellular adhesin (43, 64). Together, these data suggest that TCA cycle-dependent regulation of polysaccharide intercellular adhesin synthesis is common to the staphylococci and not just *S. epidermidis*. While amino sugar biosynthesis was increased during oxygen- and iron-limited growth, *S. aureus* acidified the culture medium irrespective of iron or oxygen availability (Fig. 1D). The latter observation is consistent with previous observations of staphylococcal carbohydrate catabolism (27, 65, 66) yet is inconsistent with more recent speculation (26).

As stated above, the metabolic perturbations during iron- and/or oxygen-limited cultivation are greatest in the post-exponential growth phase (Fig. 3A and B). These differences are primarily a consequence of the following three factors: (i) the TCA cycle is catabolite repressed during the exponential growth phase (27), (ii) derepression of the TCA cycle creates a large demand for iron in the post-exponential growth phase (Fig. 1F) (5), and (iii)

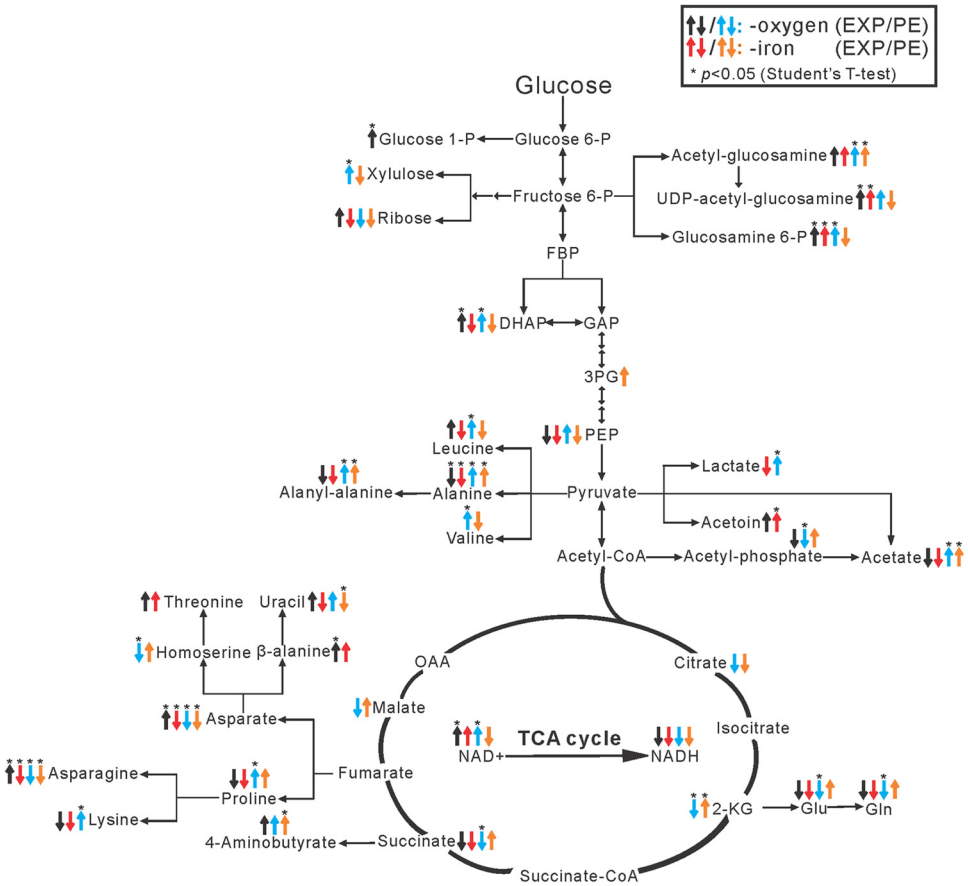

FIG 6 Schematic representation of the central metabolic changes associated with iron or oxygen limitation. The black and blue arrows indicate exponential/post-exponential-growth-phase (EXP/PE) increases or decreases in intracellular concentrations of metabolites in strain SA564 cultivated in TSB with a 10:8 flask-to-medium ratio relative to a control culture grown in TSB with a flask-to-medium ratio of 10:1. The red and orange arrows indicate exponential/post-exponential-growth-phase increases or decreases in intracellular concentrations of metabolites in strain SA564 grown in DTSB with a flask-to-medium ratio of 10:1 relative to a control culture of *S. aureus* strain SA564 grown in TSB with a flask-to-medium ratio of 10:1. Statistical significance at the 95% confidence level ($P < 0.05$) is denoted by asterisks above the arrows. Glucose-1-P, glucose-1-phosphate; FBP, fructose-1,6-bisphosphate; DHAP, dihydroxyacetone phosphate; GAP, glyceraldehyde-3-phosphate; 3PG, 3-phosphoglycerate; OAA, oxaloacetate; 2-KG, α-ketoglutarate.

TCA cycle activity generates reducing potential, which creates a need for an electron acceptor, most commonly oxygen. Once glucose is depleted from the culture medium during growth under iron- and oxygen-replete conditions (Fig. 1B), catabolite repression of the TCA cycle genes is relieved, and enzymatic activities increase (Fig. 2A and B and 5). In contrast, when *S. aureus* cells are cultivated under iron- and/or oxygen-limited conditions, levels of transcription of TCA cycle genes and enzymatic activity remain low despite the depletion of glucose (Fig. 1, 2A, and 5). Although oxygen and iron are both important for post-exponential-phase growth (Fig. 1A), the availability of oxygen is the major determinant of the metabolome (Fig. 3B and 4). The absence of oxygen prevents carbon flow through the TCA cycle, decreasing the concentrations of biosynthetic intermediates and the amino acids derived from these intermediates (Fig. 2A and B and 3); specifically, levels of citric acid, succinate, α-ketoglutarate, glutamate, glutamine, aspartate, and asparagine are decreased (Fig. 4 and 6). In other words, the decreased carbon flow through the TCA cycle results in multiple amino acid auxotrophies. In addition, the decreased carbon flow through the TCA cycle likely decreased the availability of oxaloacetate/phosphoenolpyruvate (PEP) for gluconeogenesis, which is essential for growth when glucose has been depleted from the medium. Combined, the amino acid auxotrophies, a lack of gluconeogenesis, and the inhibition of the electron transport chain (i.e., due to the lack of an electron acceptor) result in a decreased growth yield (Fig. 1A).

Inhibition of electron transport forces bacteria to use alternative pathways to oxidize dinucleotides; however, these alternatives are strongly dependent upon carbon availability. When carbon sources that can generate pyruvate (e.g., glucose and serine) are abundant in the medium, bacteria can maintain redox balance by using enzymes like lactate dehydrogenase, which leads to the accumulation of lactic acid in the medium (Fig. 1F and 4). In addition to lactate dehydrogenase, *S. aureus* can oxidize dinucleotides through alanine dehydrogenase, a result consistent with the post-exponential-growth-phase accumulation of D-alanyl–D-alanine and alanine. These data suggest that as readily catabolizable carbon sources are being depleted from the medium, several pathways are used to oxidize dinucleotides, resulting in an accumulation of NAD^+ (Fig. 4). While oxidation of dinucleotides is important, it is only one part of redox homeostasis, the other being reduction.

When the TCA cycle is inhibited by iron and/or oxygen limitation, the ability to reduce dinucleotides and restore redox balance is also greatly impaired. This inability to reduce dinucleotides is reflected in the decreased concentrations of TCA cycle-associated metabolites and amino acids, namely, aspartate asparagine, citrate, succinate, α-ketoglutarate, glutamate, and glutamine. In addition to the TCA cycle, glycerol-3-phosphate can be used in an electron transfer reaction to reduce NAD^+ to NADH and generate dihydroxyacetone phosphate. This reduction reaction is consistent with the oxygen-limited accumulation of dihydroxyacetone (the phosphate is labile and can be lost during harvest and sample preparation to generate the more stable dihydroxyacetone) (Fig. 4). When carbon flow through the TCA cycle and pentose phosphate pathway is decreased, the ability to generate reducing potential via the NAD(P)H-dependent glycerol-3-phosphate dehydrogenase (Fig. 4) can be important for redox homeostasis and biosynthesis. That being said, this metabolic rearrangement is insufficient to offset the accumulation of NAD^+. In summary, the necessity of maintaining redox homeostasis explains why the availability of oxygen (i.e., its function as an electron acceptor) has a greater influence on the post-exponential-growth-phase metabolome than does the availability of iron (Fig. 3B). In the absence of an electron acceptor, iron is not needed for electron transport; hence, the demand for iron is lower. This also explains why oxygen availability alters the transcription of genes involved in iron acquisition (Fig. 5). In essence, decreased oxygen availability suppresses the iron-sparing response, a phenomenon similar to that seen in *Saccharomyces cerevisiae* (67).

ACKNOWLEDGMENTS

G.A.S. was supported by funds provided through the Hatch Act to the University of Nebraska Institute of Agriculture and Natural Resources and by funds provided through the National Institutes of Health (grant AI087668) to G.A.S. and R.P. R.P. was supported by funds provided through the NIH (grants P20 RR-17675 and P30 GM103335) and from the American Heart Association (grant 0860033Z). Portions of this research were performed in facilities renovated with support from the NIH (grant RR015468-01).

REFERENCES

1. **Vandenesch F, Kornblum J, Novick RP.** 1991. A temporal signal, independent of agr, is required for hla but not spa transcription in *Staphylococcus aureus*. J. Bacteriol. **173:**6313–6320.
2. **Richardson AR, Libby SJ, Fang FC.** 2008. A nitric oxide-inducible lactate dehydrogenase enables *Staphylococcus aureus* to resist innate immunity. Science **319:**1672–1676. http://dx.doi.org/10.1126/science.1155207.
3. **Somerville GA, Proctor RA.** 2009. At the crossroads of bacterial metabolism and virulence factor synthesis in staphylococci. Microbiol. Mol. Biol. Rev. **73:**233–248. http://dx.doi.org/10.1128/MMBR.00005-09.
4. **Somerville GA, Chaussee MS, Morgan CI, Fitzgerald JR, Dorward DW, Reitzer LJ, Musser JM.** 2002. *Staphylococcus aureus* aconitase inactivation unexpectedly inhibits post-exponential-phase growth and enhances stationary-phase survival. Infect. Immun. **70:**6373–6382. http://dx.doi.org/10.1128/IAI.70.11.6373-6382.2002.
5. **Somerville GA, Cockayne A, Dürr M, Peschel A, Otto M, Musser JM.** 2003. Synthesis and deformylation of *Staphylococcus aureus* delta-toxin are linked to tricarboxylic acid cycle activity. J. Bacteriol. **185:**6686–6694. http://dx.doi.org/10.1128/JB.185.22.6686-6694.2003.
6. **Majerczyk CD, Dunman PM, Luong TT, Lee CY, Sadykov MR, Somerville GA, Bodi K, Sonenshein AL.** 2010. Direct targets of CodY in *Staphylococcus aureus*. J. Bacteriol. **192:**2861–2877. http://dx.doi.org/10.1128/JB.00220-10.
7. **Sadykov MR, Hartmann T, Mattes TA, Hiatt M, Jann NJ, Zhu Y, Ledala N, Landmann R, Herrmann M, Rohde H, Bischoff M, Somerville GA.** 2011. CcpA coordinates central metabolism and biofilm formation in *Staphylococcus epidermidis*. Microbiology **157:**3458–3468. http://dx.doi.org/10.1099/mic.0.051243-0.
8. **Zhu Y, Nandakumar R, Sadykov MR, Madayiputhiya N, Luong TT, Gaupp R, Lee CY, Somerville GA.** 2011. RpiR homologues may link *Staphylococcus aureus* RNAIII synthesis and pentose phosphate pathway regulation. J. Bacteriol. **193:**6187–6196. http://dx.doi.org/10.1128/JB.05930-11.
9. **Majerczyk CD, Sadykov MR, Luong TT, Lee C, Somerville GA, Sonenshein AL.** 2008. *Staphylococcus aureus* CodY negatively regulates virulence gene expression. J. Bacteriol. **190:**2257–2265. http://dx.doi.org/10.1128/JB.01545-07.
10. **Pohl K, Francois P, Stenz L, Schlink F, Geiger T, Herbert S, Goerke C, Schrenzel J, Wolz C.** 2009. CodY in *Staphylococcus aureus*: a regulatory link between metabolism and virulence gene expression. J. Bacteriol. **191:**2953–2963. http://dx.doi.org/10.1128/JB.01492-08.
11. **Deutscher J, Kuster E, Bergstedt U, Charrier V, Hillen W.** 1995. Protein kinase-dependent HPr/CcpA interaction links glycolytic activity to carbon catabolite repression in gram-positive bacteria. Mol. Microbiol. **15:**1049–1053. http://dx.doi.org/10.1111/j.1365-2958.1995.tb02280.x.
12. **Seidl K, Stucki M, Ruegg M, Goerke C, Wolz C, Harris L, Berger-Bächi B, Bischoff M.** 2006. *Staphylococcus aureus* CcpA affects virulence determinant production and antibiotic resistance. Antimicrob. Agents Chemother. **50:**1183–1194. http://dx.doi.org/10.1128/AAC.50.4.1183-1194.2006.
13. **Jaeger T, Mayer C.** 2008. The transcriptional factors MurR and catabolite activator protein regulate N-acetylmuramic acid catabolism in *Escherichia coli*. J. Bacteriol. **190:**6598–6608. http://dx.doi.org/10.1128/JB.00642-08.
14. **Shivers RP, Sonenshein AL.** 2004. Activation of the *Bacillus subtilis* global regulator CodY by direct interaction with branched-chain amino acids. Mol. Microbiol. **53:**599–611. http://dx.doi.org/10.1111/j.1365-2958.2004.04135.x.
15. **Romling U, Galperin MY, Gomelsky M.** 2013. Cyclic di-GMP: the first 25 years of a universal bacterial second messenger. Microbiol. Mol. Biol. Rev. **77:**1–52. http://dx.doi.org/10.1128/MMBR.00043-12.
16. **Ernst JF, Bennett RL, Rothfield LI.** 1978. Constitutive expression of the iron-enterochelin and ferrichrome uptake systems in a mutant strain of *Salmonella typhimurium*. J. Bacteriol. **135:**928–934.
17. **Sadykov MR, Zhang B, Halouska S, Nelson JL, Kreimer LW, Zhu Y, Powers R, Somerville GA.** 2010. Using NMR metabolomics to investigate tricarboxylic acid cycle dependent signal transduction in *Staphylococcus epidermidis*. J. Biol. Chem. **285:**36616–36624. http://dx.doi.org/10.1074/jbc.M110.152843.
18. **Zhang B, Halouska S, Schiaffo CE, Sadykov MR, Somerville GA, Powers R.** 2011. NMR analysis of a stress response metabolic signaling network. J. Proteome Res. **10:**3743–3754. http://dx.doi.org/10.1021/pr200360w.
19. **Cohen S, Sweeney HM, Leitner F.** 1967. Relation between iron uptake, pH of growth medium, and penicillinase formation in *Staphylococcus aureus*. J. Bacteriol. **93:**1227–1235.
20. **Johnson M, Cockayne A, Morrissey JA.** 2008. Iron-regulated biofilm formation in *Staphylococcus aureus* Newman requires *ica* and the secreted protein Emp. Infect. Immun. **76:**1756–1765. http://dx.doi.org/10.1128/IAI.01635-07.
21. **Trivier D, Courcol RJ.** 1996. Iron depletion and virulence in *Staphylococcus aureus*. FEMS Microbiol. Lett. **141:**117–127. http://dx.doi.org/10.1111/j.1574-6968.1996.tb08373.x.
22. **Dassy B, Fournier JM.** 1996. Respiratory activity is essential for post-exponential-phase production of type 5 capsular polysaccharide by *Staphylococcus aureus*. Infect. Immun. **64:**2408–2414.
23. **Jacobs NJ, Maclosky ER, Conti SF.** 1967. Effects of oxygen and heme on the development of a microbial respiratory system. J. Bacteriol. **93:**278–285.
24. **Ferreira MT, Manso AS, Gaspar P, Pinho MG, Neves AR.** 2013. Effect of oxygen on glucose metabolism: utilization of lactate in *Staphylococcus aureus* as revealed by in vivo NMR studies. PLoS One **8:**e58277. http://dx.doi.org/10.1371/journal.pone.0058277.
25. **Fuchs S, Pané-Farré J, Kohler C, Hecker M, Engelmann S.** 2007. Anaerobic gene expression in *Staphylococcus aureus*. J. Bacteriol. **189:**4275–4289. http://dx.doi.org/10.1128/JB.00081-07.
26. **Friedman DB, Stauff DL, Pishchany G, Whitwell CW, Torres VJ, Skaar EP.** 2006. *Staphylococcus aureus* redirects central metabolism to increase iron availability. PLoS Pathog. **2:**e87. http://dx.doi.org/10.1371/journal.ppat.0020087.
27. **Somerville GA, Saïd-Salim B, Wickman JM, Raffel SJ, Kreiswirth BN,**

Musser JM. 2003. Correlation of acetate catabolism and growth yield in *Staphylococcus aureus*: implications for host-pathogen interactions. Infect. Immun. **71:**4724–4732. http://dx.doi.org/10.1128/IAI.71.8.4724-4732.2003.
28. **Sheppard LN, Kontoghiorghes GJ.** 1993. Competition between deferiprone, desferrioxamine and other chelators for iron and the effect of other metals. Arzneimittelforschung **43:**659–663.
29. **Somerville GA, Proctor RA.** 2013. Cultivation conditions and the diffusion of oxygen into culture media: the rationale for the flask-to-medium ratio in microbiology. BMC Microbiol. **13:**9. http://dx.doi.org/10.1186/1471-2180-13-9.
30. **Zhang B, Halouska S, Gaupp R, Lei S, Snell E, Fenton RJ, Barletta RG, Somerville GA, Powers R.** 2013. Revisiting protocols for the NMR analysis of bacterial metabolomes. J. Integr. OMICS **3:**120–137. http://dx.doi.org/10.5584/jiomics.v3i2.139.
31. **Hu K, Westler WM, Markley JL.** 2011. Simultaneous quantification and identification of individual chemicals in metabolite mixtures by two-dimensional extrapolated time-zero (1)H-(13)C HSQC (HSQC(0)). J. Am. Chem. Soc. **133:**1662–1665. http://dx.doi.org/10.1021/ja1095304.
32. **Delaglio F, Grzesiek S, Vuister GW, Zhu G, Pfeifer J, Bax A.** 1995. NMRPipe: a multidimensional spectral processing system based on UNIX pipes. J. Biomol. NMR **6:**277–293.
33. **Downlinging A.** 2004. Using NMRView to visualize and analyze the NMR spectra of macromolecules, p 40. *In* Johnson BA (ed), Protein NMR techniques, vol 278. Humana Press, Inc, Totowa, NJ.
34. **Shao J.** 1993. Linear model selection by cross-validation. J. Am. Stat. Assoc. **88:**486–494. http://dx.doi.org/10.1080/01621459.1993.10476299.
35. **Golbraikh A, Tropsha A.** 2002. Beware of q2! J. Mol. Graph. Model. **20:**269–276. http://dx.doi.org/10.1016/S1093-3263(01)00123-1.
36. **Eriksson L, Trygg J, Wold S.** 2008. CV-ANOVA for significance testing of PLS and OPLS models. J. Chemom. **22:**594–600. http://dx.doi.org/10.1002/cem.1187.
37. **Werth MT, Halouska S, Shortridge MD, Zhang B, Powers R.** 2010. Analysis of metabolomic principal component analysis data using tree diagrams. Anal. Biochem. **399:**58–63. http://dx.doi.org/10.1016/j.ab.2009.12.022.
38. **Worley B, Halouska S, Powers R.** 2013. Utilities for quantifying separation in PCA/PLS-DA scores plots. Anal. Biochem. **433:**102–104. http://dx.doi.org/10.1016/j.ab.2012.10.011.
39. **Wishart DS, Knox C, Guo AC, Eisner R, Young N, Gautam B, Hau DD, Psychogios N, Dong E, Bouatra S, Mandal R, Sinelnikov I, Xia J, Jia L, Cruz JA, Lim E, Sobsey CA, Shrivastava S, Huang P, Liu P, Fang L, Peng J, Fradette R, Cheng D, Tzur D, Clements M, Lewis A, De Souza A, Zuniga A, Dawe M, Xiong Y, Clive D, Greiner R, Nazyrova A, Shaykhutdinov R, Li L, Vogel HJ, Forsythe I.** 2009. HMDB: a knowledgebase for the human metabolome. Nucleic Acids Res. **37:**D603–D610. http://dx.doi.org/10.1093/nar/gkn810.
40. **Akiyama K, Chikayama E, Yuasa H, Shimada Y, Tohge T, Shinozaki K, Hirai MY, Sakurai T, Kikuchi J, Saito K.** 2008. PRIMe: a Web site that assembles tools for metabolomics and transcriptomics. In Silico Biol. **8:**339–345.
41. **Markley JL, Ulrich EL, Berman HM, Henrick K, Nakamura H, Akutsu H.** 2008. BioMagResBank (BMRB) as a partner in the Worldwide Protein Data Bank (wwPDB): new policies affecting biomolecular NMR depositions. J. Biomol. NMR **40:**153–155. http://dx.doi.org/10.1007/s10858-008-9221-y.
42. **Team RDC.** 2011. R: a language and environment for statistical computing. R Foundation for Statistical Computing, Vienna, Austria.
43. **Sadykov MR, Olson ME, Halouska S, Zhu Y, Fey PD, Powers R, Somerville GA.** 2008. Tricarboxylic acid cycle-dependent regulation of *Staphylococcus epidermidis* polysaccharide intercellular adhesin synthesis. J. Bacteriol. **190:**7621–7632. http://dx.doi.org/10.1128/JB.00806-08.
44. **Fox JB, Holtman DF.** 1968. Effect of anaerobiosis on staphylococcal nuclease production. J. Bacteriol. **95:**1548–1550.
45. **Theodore TS, Schade AL.** 1965. Carbohydrate metabolism of iron-rich and iron-poor *Staphylococcus aureus*. J. Gen. Microbiol. **40:**385–395. http://dx.doi.org/10.1099/00221287-40-3-385.
46. **Theodore TS, Schade AL.** 1965. Growth of *Staphylococcus aureus* in media of restricted and unrestricted inorganic iron availability. J. Gen. Microbiol. **39:**75–83. http://dx.doi.org/10.1099/00221287-39-1-75.
47. **Pasteur L.** 1861. Animalcules infusoires vivant sans gaz oxygene libre et determinant des fermentations. Compt. Rend. Acad. Sci. (Paris) **52:**344–347.
48. **Kendall AI, Friedemann TE, Ishikawa M.** 1930. Quantitative observations on the chemical activity of "resting" *Staphylococcus aureus*. J. Infect. Dis. **47:**223–228. http://dx.doi.org/10.1093/infdis/47.3.223.
49. **Krebs HA.** 1937. Dismutation of pyruvic acid in *Gonococcus* and *Staphylococcus*. Biochem. J. **31:**661–671.
50. **Gardner JF, Lascelles J.** 1962. The requirement for acetate of a streptomycin-resistant strain of *Staphylococcus aureus*. J. Gen. Microbiol. **29:**157–164. http://dx.doi.org/10.1099/00221287-29-1-157.
51. **Fuller JR, Vitko NP, Perkowski EF, Scott E, Khatri D, Spontak JS, Thurlow LR, Richardson AR.** 2011. Identification of a lactate-quinone oxidoreductase in *Staphylococcus aureus* that is essential for virulence. Front. Cell. Infect. Microbiol. **1:**19. http://dx.doi.org/10.3389/fcimb.2011.00019.
52. **Goldschmidt MC, Powelson DM.** 1953. Effect of the culture medium on the oxidation of acetate by *Micrococcus pyogenes* var. *aureus*. Arch. Biochem. Biophys. **46:**154–163. http://dx.doi.org/10.1016/0003-9861(53)90178-7.
53. **Bylesjo M, Rantalainen M, Cloarec O, Nicholson JK, Holmes E, Trygg J.** 2006. OPLS discriminant analysis: combining the strengths of PLS-DA and SIMCA classification. J. Chemom. **20:**341–351. http://dx.doi.org/10.1002/cem.1006.
54. **Beasley FC, Cheung J, Heinrichs DE.** 2011. Mutation of L-2,3-diaminopropionic acid synthase genes blocks staphyloferrin B synthesis in *Staphylococcus aureus*. BMC Microbiol. **11:**199. http://dx.doi.org/10.1186/1471-2180-11-199.
55. **Morrissey JA, Cockayne A, Hill PJ, Williams P.** 2000. Molecular cloning and analysis of a putative siderophore ABC transporter from *Staphylococcus aureus*. Infect. Immun. **68:**6281–6288. http://dx.doi.org/10.1128/IAI.68.11.6281-6288.2000.
56. **Knobloch JK, Bartscht K, Sabottke A, Rohde H, Feucht HH, Mack D.** 2001. Biofilm formation by *Staphylococcus epidermidis* depends on functional RsbU, an activator of the *sigB* operon: differential activation mechanisms due to ethanol and salt stress. J. Bacteriol. **183:**2624–2633. http://dx.doi.org/10.1128/JB.183.8.2624-2633.2001.
57. **Mack D, Siemssen N, Laufs R.** 1992. Parallel induction by glucose of adherence and a polysaccharide antigen specific for plastic-adherent *Staphylococcus epidermidis*: evidence for functional relation to intercellular adhesion. Infect. Immun. **60:**2048–2057.
58. **Deighton M, Borland R.** 1993. Regulation of slime production in *Staphylococcus epidermidis* by iron limitation. Infect. Immun. **61:**4473–4479.
59. **Rachid S, Ohlsen K, Witte W, Hacker J, Ziebuhr W.** 2000. Effect of subinhibitory antibiotic concentrations on polysaccharide intercellular adhesin expression in biofilm-forming *Staphylococcus epidermidis*. Antimicrob. Agents Chemother. **44:**3357–3363. http://dx.doi.org/10.1128/AAC.44.12.3357-3363.2000.
60. **Nychas GJ, Tranter HS, Brehm RD, Board RG.** 1991. *Staphylococcus aureus* S-6: factors affecting its growth, enterotoxin B production and exoprotein formation. J. Appl. Bacteriol. **70:**344–350. http://dx.doi.org/10.1111/j.1365-2672.1991.tb02947.x.
61. **Seidl K, Müller S, Francois P, Kriebitzsch C, Schrenzel J, Engelmann S, Bischoff M, Berger-Bächi B.** 2009. Effect of a glucose impulse on the CcpA regulon in *Staphylococcus aureus*. BMC Microbiol. **9:**95. http://dx.doi.org/10.1186/1471-2180-9-95.
62. **Ulrich M, Bastian M, Cramton SE, Ziegler K, Pragman AA, Bragonzi A, Memmi G, Wolz C, Schlievert PM, Cheung A, Döring G.** 2007. The staphylococcal respiratory response regulator SrrAB induces *ica* gene transcription and polysaccharide intercellular adhesin expression, protecting *Staphylococcus aureus* from neutrophil killing under anaerobic growth conditions. Mol. Microbiol. **65:**1276–1287. http://dx.doi.org/10.1111/j.1365-2958.2007.05863.x.
63. **Neidhardt FC.** 2006. Apples, oranges and unknown fruit. Nat. Rev. Microbiol. **4:**876. http://dx.doi.org/10.1038/nrmicro1554.
64. **Vuong C, Kidder JB, Jacobson ER, Otto M, Proctor RA, Somerville GA.** 2005. *Staphylococcus epidermidis* polysaccharide intercellular adhesin production significantly increases during tricarboxylic acid cycle stress. J. Bacteriol. **187:**2967–2973. http://dx.doi.org/10.1128/JB.187.9.2967-2973.2005.
65. **Blumenthal HJ.** 1972. Glucose catabolism in staphylococci, p 111–135. *In* Cohen JO (ed), The staphylococci. Wiley Interscience, New York, NY.
66. **Elek SD.** 1959. *Staphylococcus pyogenes* and its relation to disease, p 54–105. E & S Livingstone Ltd, London, United Kingdom.

67. **Kaplan J, McVey Ward D, Crisp RJ, Philpott CC.** 2006. Iron-dependent metabolic remodeling in *S. cerevisiae*. Biochim. Biophys. Acta **1763:**646–651. http://dx.doi.org/10.1016/j.bbamcr.2006.03.008.
68. **Kuroda M, Ohta T, Uchiyama I, Baba T, Yuzawa H, Kobayashi I, Cui L, Oguchi A, Aoki K, Nagai Y, Lian J, Ito T, Kanamori M, Matsumaru H, Maruyama A, Murakami H, Hosoyama A, Mizutani-Ui Y, Takahashi NK, Sawano T, Inoue R, Kaito C, Sekimizu K, Hirakawa H, Kuhara S, Goto S, Yabuzaki J, Kanehisa M, Yamashita A, Oshima K, Furuya K, Yoshino C, Shiba T, Hattori M, Ogasawara N, Hayashi H, Hiramatsu K.** 2001. Whole genome sequencing of meticillin-resistant *Staphylococcus aureus*. Lancet **357:**1225–1240. http://dx.doi.org/10.1016/S0140-6736(00)04403-2.

Supplemental table 1. Summary of metabolite changes [a]

Culture conditions	TSB, 10:8		DTSB, 10:1		DTSB, 10:8		Metabolite	Metabolic Pathway
Growth phase	Exp	PE	Exp	PE	Exp	PE	KEGG ID	KEGG ID
Xanthosine					↓		C01762	00230, 01065
Uracil				↓			C00106	00240,00410,00770
UDPAcGlcN	↑↑		↑↑↑		↑		C00043	00520, 00540,00550
Succinate		↓↓↓				↓↓↓	C00042	00020,00190,00250,00350,00360 ,00630,00650,02020
Proline		↑				↑↑↑	C00148	00330,00970 ,01230,02010
NAD^+	↑↑	↑↑↑				↑↑	C00003	00190
Lysine		↑↑↑				↑	C00047	00300,00310,00780, 00970,01210,01230,02010
Lactate		↑↑↑				↑	C00186	00010,00620,00640
GPC			↓	↓		↓	C00670	00564,00565
Glyceraldehyde				↓		↓	C00577	00030,00051,00561
Glutamine		↓↓↓				↓↓↓	C00064	00230,00240,00250,00330,00471,00970,01230,02010,02020
Glutamate		↓↓↓				↓↓↓	C00025	00250,00330,00340,00430,00471,00480,00650,00660,00970,01210, 01230,02010,02020
Glc6P	↑	↑↑↑	↑			↑↑↑	C00352	00250,00520,02060
Dihydroxyacetone	↑↑	↑↑↑				↑↑↑	C00184	00561,00680
Betaine	↓↓		↓	↑↑	↓↓	↑↑	C00719	00260,02010
Aspartate	↑↑	↓↓↓	↓	↓↓			C00049	00250,00260,00270,00300,00330,00340,00410,00770,00970,01210, 01230,02010,02020
Asparagine	↑↑↑	↓↓↓	↓↓↓	↓↓↓	↓↓↓	↓↓↓	C00152	00250,00970,01230
Alanyl-alanine		↑↑		↑↑	↓	↑↑↑	C00993	00473,00550
Alanine	↓	↑↑↑	↓↓	↑↑	↓↓	↑↑↑	C00041	00250,00270,00430 ,00473,00970,01230,02010
Acetyl-phosphate		↓↓			↓	↓↓	C00227	00430,00620,00680
Acetyl-glucosamine		↑↑↑		↑↑			C00140	00520, 01110,02010,02060
Acetate		↑↑		↑↑		↑↑↑	C00033	00010,00430,00440,00534,00620,00660,00680
4-Aminobutyrate				↑↑		↑↑	C00334	00250,00330,00410,00650
2-Hydroxyglutarate		↓↓↓		↑			C00026	00020,00040,00053,00250,00300,00340,00430,00471,00650,00660, 01210,01230

[a] "↑" indicates an increase; "↓" indicates a decrease. One arrow represents a $p \leq 0.05$ (Student's T-test), two arrows represents a $p \leq 0.01$, three arrows represents a $p \leq 0.001$.

[b]Metabolites altered in the exponential (Exp) growth phase in TSB, 10:8, DTSB,10:1 and DTSB10:8 relative to the cultures grown in TSB with a 10:1 flask-to-medium ratio.

[c]Metabolites altered in the post-exponential phase (PE) of growth in TSB, 10:8, DTSB,10:1 and DTSB10:8 relative to the cultures grown in TSB with a 10:1 flask-to-medium ratio.

8 [d]KEGG (Kyoto Encyclopedia of Genes and Genomes) database identification number for the metabolite and the associate metabolic pathways.

Supplemental Figure1.

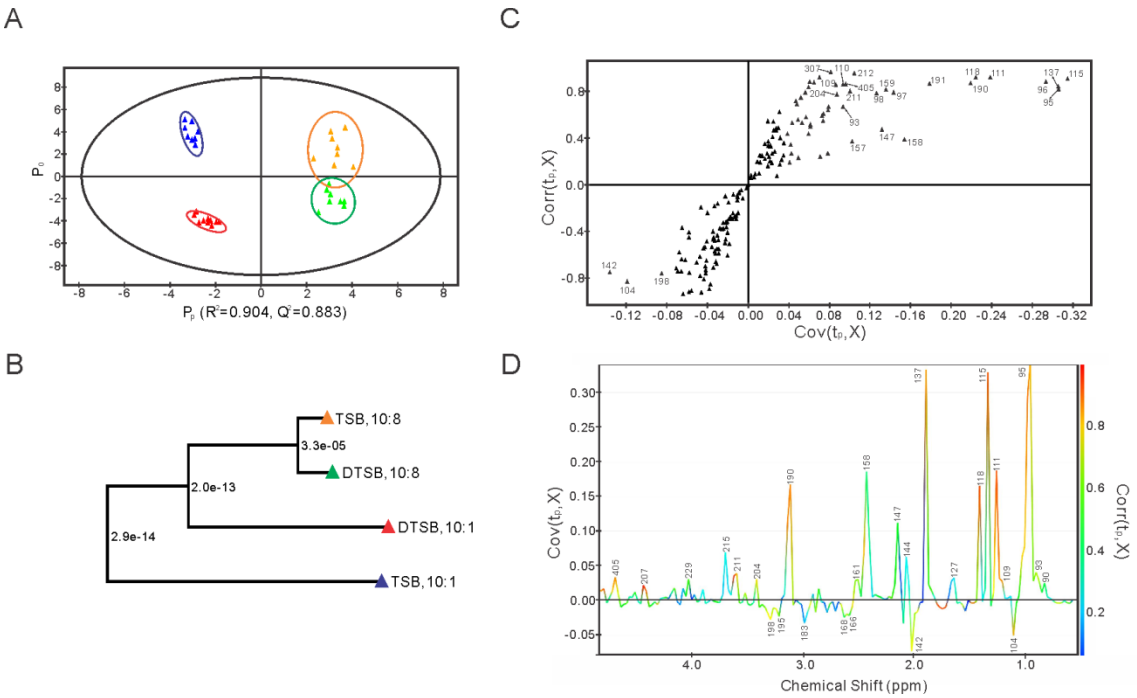

Figure S1. (A) OPLS-DA scores plot generated from 1D ^{1}H NMR spectra of iron- and/or aeration-limited cultures of *S. aureus* strain SA564 in the exponential (2 h) growth phase. The ellipses in the OPLS-DA scores plot correspond to the 95% confidence limits from a normal distribution for each cluster. TSB, 10:1 (▲); DTSB, 10:1 (▲); TSB, 10:8 (▲); DTSB, 10:8 (▲). (B) Metabolic tree generated using the OPLS-DA data demonstrating the relationship of iron- and/or oxygen-limited cultures in the exponential growth phase. (C) S-plot identifies the chemical shift bins that significantly contribute to class separation in the OPLS-DA scores plot. (D) OPLS-DA loading plot comparing two aeration conditions 10:1 and 10:8 for *S. aureus* strain SA564 grown on either TSB or DTSB media. Negative values indicate a decrease in peak intensity when comparing 10:8 to 10:1, while positive values indicate an increase in peak intensity. The color scale on the right indicates the relative correlation of the data to the OPLS-DA model and class separation.

Supplemental Figure 2.

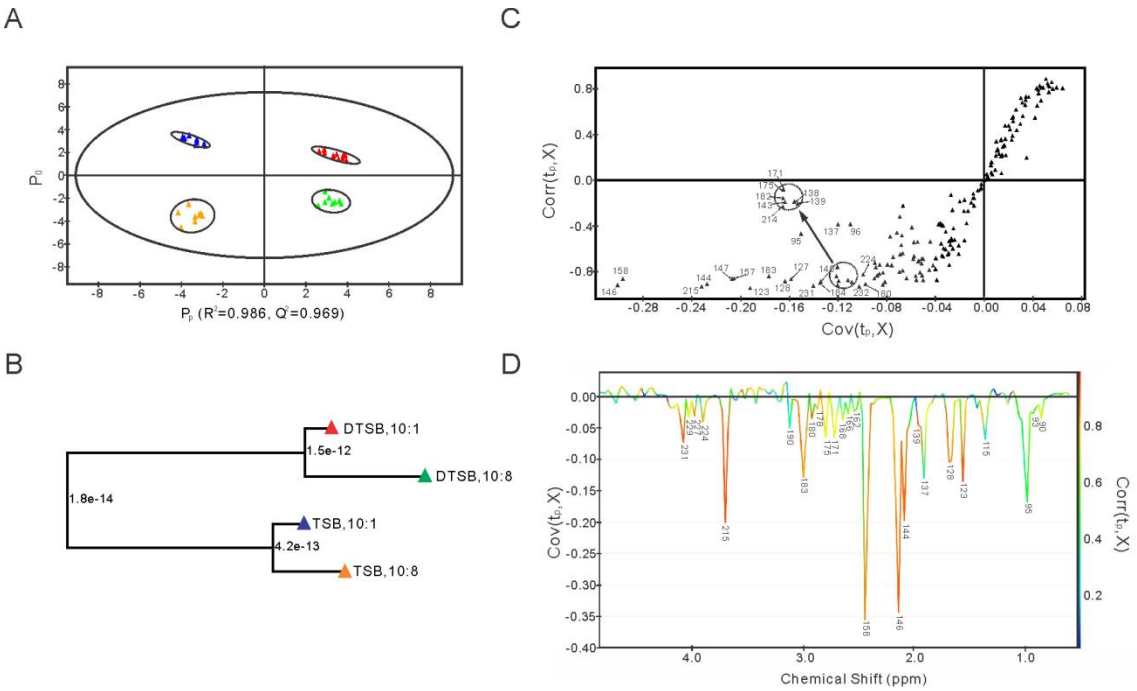

Figure S2. (A) OPLS-DA scores plot generated from 1D ^{1}H NMR spectra of iron- and/or aeration-limited cultures of *S. aureus* strain SA564 in the post-exponential (6 h) growth phase. The ellipses in the OPLS-DA scores plot correspond to the 95% confidence limits from a normal distribution for each cluster. TSB, 10:1 (▲); DTSB, 10:1 (▲); TSB, 10:8 (▲); DTSB, 10:8 (▲). (B) Metabolic tree generated using the OPLS-DA data demonstrating the relationship of iron- and/or oxygen-limited cultures in the exponential growth phase. (C) S-plot identifies the chemical shift bins that significantly contribute to class separation in the OPLS-DA scores plot. (D) OPLS-DA loading plot comparing two aeration conditions 10:1 and 10:8 for *S. aureus* strain SA564 grown on either TSB or DTSB media. Negative values indicate a decrease in peak intensity when comparing DTSB media to TSB media, while positive values indicate an increase in peak intensity. The color scale on the right indicates the relative correlation of the data to the OPLS-DA model and class separation.